Environ Geochem Health (2026) 48:628
https://doi.org/10.1007/s10653-026-03515-y

ORIGINAL PAPER

Geopolymer fungal cell integration achieved through passive immobilization: a new sustainable candidate to effectively remove toxic lead contamination

Tamer Akar · Fatih Sayin · Sibel Tunali Akar · Ilknur Kara · Sema Celik · Halime Çınar · Gülşah Özen · Ferhat Kara

Received: 18 April 2026 / Accepted: 25 September 2026
© The Author(s), under exclusive licence to Springer Nature B.V. 2026

Abstract The novel hybrid sorbent (JEONS5), developed with *Neurospora* cells immobilized on a geopolymer support, is proposed for the removal of toxic Pb^{2+} ions. The investigation focused on sorbent characterization and the potential sorbent-pollutant interactions utilizing zeta potential measurements, infrared spectroscopy (FTIR), scanning electron microscopy (SEM) combined with Energy-dispersive X-ray spectroscopy (EDX), X-ray diffraction (XRD), X-ray fluorescence (XRF), and X-ray photoelectron spectroscopy (XPS). During the sorption process, the joint activity of the geopolymer and *Neurospora* cells was noted. The groups –OH, –NH, C=O, C–N, Si–O, and Al–O were found to have the potential to be efficient. For effective Pb^{2+} uptake (> 95%) in batch mode, the optimal pH and JEONS5 dosage were determined to be 5.0 and 0.04 g, respectively, using a metal ion concentration of 100 mg L^{-1}. The uptake was very rapid and independent of temperature; equilibrium was reached in approximately 30 min, with more than 75% of the total uptake occurring within the first 5 min. The Langmuir model proved more suitable for the equilibrium data with a q_{max} of 1.05×10^{-3} mol g^{-1} (217.56 mg g^{-1}), even if the pseudo-second-order kinetic model fitted the sorption kinetics well. Breakthrough and exhaustion points were noted at 20 and 350 min. The JEONS5 column's breakthrough curve is fairly well fitted by Chu's simplistic model. Regeneration tests have shown that JEONS5 exhibited sorption and desorption efficiencies exceeding 90% in the first ten cycles, and even at the end of the 20th cycle, it could still demonstrate 50% sorption efficiency. Mechanistic studies indicate that the Pb^{2+} sorption process proceeds via several concurrent pathways, including surface complexation, ion exchange, and electrostatic interactions. Our findings argue that JEONS5 has enormous potential for treating toxic Pb^{2+}-contaminated aquatic systems.

Keywords Geopolymer support · Composite sorbent · Immobilization · Metal sorption · Application

Supplementary Information The online version contains supplementary material available at https://doi.org/10.1007/s10653-026-03515-y.

T. Akar (✉) · F. Sayin · S. Tunali Akar · S. Celik
Department of Chemistry, Faculty of Science, Eskişehir Osmangazi University, 26040 Eskişehir, Türkiye
e-mail: takar@ogu.edu.tr

H. Çınar · G. Özen
Department of Chemistry, Graduate School of Natural and Applied Sciences, Eskişehir Osmangazi University, 26040 Eskişehir, Türkiye

I. Kara
Department of Elementary Education, Faculty of Education, Anadolu University, 26470 Eskişehir, Türkiye

F. Kara
Department of Materials Science and Engineering, Faculty of Engineering, Eskişehir Technical University, İki Eylül Campus, 26555 Eskişehir, Türkiye

Published online: 08 October 2026

Content courtesy of Springer Nature, terms of use apply. Rights reserved.

Introduction

The availability of freshwater resources is drastically declining today, even though demand for them is continuously rising. Human-caused water pollution, also linked to global climate change, affects all living things and requires urgent and practical solutions. Public health depends on preventing pollution and using this valuable resource-which is the foundation of life-in a sustainable manner (Adebesin et al., 2018; Kümmerer et al., 2018).

Transporting different pollutants, primarily heavy metal ions, from poorly treated wastewater going to receiving water sources from a wide range of industries, including chemical production, metallurgy, mining, battery manufacturing, and the pharmaceutical industry, is currently one of the biggest challenges (Verma et al., 2021). Heavy metals have a high toxicity potential, are non-biodegradable, can accumulate in the food chain, exhibit a strong tendency to bioaccumulate in living organisms, and are extremely difficult to eliminate through metabolic processes. These toxicities are mostly linked to significant harm to some tissues, particularly the digestive, reproductive, and neurological systems. The fact that the metabolic damage they cause through inhibition and induction can lead to cell death clearly highlights the importance of effectively removing heavy metals from contaminated sources (Gupta et al., 2012). Lead, a common industrial heavy metal contaminant, is part of the "big three of metals" with the highest risk of toxicity, along with mercury and cadmium (Volesky, 1990). Effective treatment of water contaminated with heavy metals is currently a major topic of research to reduce the likelihood of these health impacts.

Research is progressing rapidly to find novel, ecologically friendly, and sustainable alternatives to traditional wastewater treatment techniques in order to overcome problems including high process costs, chemical inputs, and possible environmental damage. The hybrid sorbent systems, currently developed by incorporating immobilization techniques into the biosorbent design process, have attracted increasing attention (Çelik et al., 2017). The design of immobilized biomaterials is also necessary for the transition of biosorbent materials from laboratory scale to industrial applications. This is because these materials allow for industrial-scale high-volume treatment (Ramteke & Gogate, 2016).

The microbial cell carrier used in the immobilization process should be non-toxic, insoluble, resistant to degradation, affordable, simple to use, and regenerable. Additionally, it needs to be appropriate for high cell mass loading (Bouabidi et al., 2019). Natural and synthetic polymeric networks and inorganic materials have been employed in this context for distinct microbial cells, and the resulting sorbent systems have been applied to a variety of water contaminants (Blaga et al., 2021; Celik et al., 2021; Das & Adholeya, 2015; Najim et al., 2024). Also, notable results have been obtained from recent research on the application of biochar materials for this purpose. Green development, on the other hand, depends on sustainability and the effective use of materials and resources. Thus, it merits more research on the modification techniques and characteristic qualities to produce the best carriers, and it may be a potential avenue for future studies. For this reason, building a promising substance to immobilize microorganisms is crucial to the advancement of these sorbent systems (Wu et al., 2022). Aluminosilicate materials condense at low temperatures in alkaline solutions to form new inorganic polymer materials known as geopolymers, a word originally proposed by Davidovits (Davidovits, 1991). Excellent mechanical strength, strong electrical qualities, low density, and high resistance to chemical and thermal attack are only a few of these materials' exceptional physical and chemical characteristics. As a result, they are widely used in many different industries, including high-tech materials, new ceramics, fire-resistant materials, innovative geopolymer cement, and civil engineering. Geopolymers are relatively new potential sorbents in wastewater treatment due to their nanoporous structure, cost-efficiency, and green credentials, in addition to these great qualities. There has been a noticeable increase in scientific research on this subject in recent years (El Alouani et al., 2024; Luhar et al., 2021).

The goal of this work was to simultaneously benefit from the superior qualities of microbial cells and geopolymers. In this regard, *Neurospora* cells were immobilized onto a geopolymer matrix to generate a sustainable and effective composite sorbent (JEONS5). To the best of our knowledge, this is the first investigation that addresses sorption of Pb^{2+} onto a geopolymer-fungal biomass composite. The critical parameters of batch and fixed-bed treatment methods were thoroughly examined. Different kinetic and

Content courtesy of Springer Nature, terms of use apply. Rights reserved.

isotherm models were used to investigate the uptake process. The characteristics of JEONS5 and the Pb^{2+}– sorbent interaction were determined by using FTIR, XRD, XPS, XRF, BET, SEM, EDX, and zeta potential techniques. Twenty consecutive sorption/desorption tests were used to evaluate the sorbent's recyclability after the breakthrough curve analysis and modeling. To assess JEONS5's feasibility, the uptake of Pb^{2+} from different real wastewaters was also examined. In addition to offering an easy pathway to sorbent production for upcoming research, the method promotes environmental sustainability by creating a hybrid sorbent that is scalable, has high uptake capacity, and is practically applicable. It is expected that the methodology used in this study may be extended to cover the creation of distinct hybrid sorbents as well as the removal of diverse pollutants.

Materials and methods

Geopolymer synthesis and fungal cells immobilization

The previously employed suspension and solidification procedure (Kara et al., 2017) was used in this investigation to generate the geopolymer to be used as a matrix in fungal immobilization. Briefly, for the geopolymer structure, the molar ratios of the oxide components $SiO_2/Al_2O_3 = 3.2$, $Na_2O/Al_2O_3 = 0.7$, $Na_2O/SiO_2 = 0.2$, and $H_2O/Na_2O = 13.8$ were used. The alkaline activator was formed by mechanically mixing sodium silicate solution (SiO_2/Na_2O = 2.1) with NaOH pellets (purity > 99%). Water and metakaolin (Al_2O_3 = 41.9%, SiO_2 = 52.9%, Fe_2O_3 = 1.1%, TiO_2 = 1.8%, and MgO = 0.2%) were subsequently added and stirred at 1000 rpm for 15 min. High-density polyethylene (HDPE) cylinders with lids were filled with geopolymer slurry and then allowed to harden at 80 °C for two hours. After the material had fully solidified, it was crushed and sieved to obtain particles of sizes ranging from 150 to 212 µm.

Ascomycete *Neurospora sitophila* (ATCC 36935), which was acquired from ATCC (The Global Bioresource Center), served as the source of fungal biomass for this investigation. Employing sterile liquid growing media (Shojaosadati et al., 1999), *N. sitophila* biomass (NS) was generated at 26 °C and 120 rpm. Erlenmeyer flasks containing 0.5 g of geopolymer matrix were filled with 100 mL (pH 5–5.5) of liquid culture media before sterilization. These flasks were sterilized for 15 min at 121 °C and then allowed to cool. Each flask was inoculated with 1 mL of the fungal spore suspension under aseptic conditions, then incubated in an orbital shaker (Gerhardt Thermoshake) for 7 days at 26 °C and 120 rpm. The immobilized biomass obtained was washed by filtration and dried at 60 °C for 12 h. Finally, it was ground again and passed through sieves to ensure that the sorbent particle size fell within the 150–212 µm range, and it was labeled as JEONS5 for further use (Fig. 1). This biomass production procedure was also employed without a geopolymer matrix to produce biomass in its free form.

Batch and continuous flow mode treatment tests

For the batch mode sorption tests, 25 mL of Pb^{2+} solutions at concentrations between 25 and 1000 mg L^{-1} were used. The JEONS5 was used in the sorption tests and had a mass of 0.01 to 0.08 g. The effect of initial solution pH on Pb^{2+} uptake by JEONS5 was investigated over the pH range of 2.0–5.0. For experiments conducted at pH 2.0–4.0, the solution pH was adjusted to the desired value using small amounts of 0.1 M HCl or 0.1 M NaOH. The experiments at pH 5.0 were performed in an acetate buffer to minimize changes in solution pH during the sorption process and to prevent possible precipitation of lead hydroxide. The acetate buffer (0.01 M) was prepared at the desired pH. The pH values of the solutions at 2.0, 3.0, 4.0, and 5.0 were recorded as 2.64, 3.95, 4.26, and 4.92, respectively, after the sorption process. The ranges of 15–35 °C and 5–90 min were used to examine the impacts of temperature and contact time, respectively. Lead solution (100 mg L^{-1}) was likewise supplied with different doses of KNO_3 in order to evaluate the impact of inorganic salts (0.01 M, 0.02 M, 0.04 M, 0.06 M, 0.08 M, and 0.1 M) on the sorptive treatment potential of JEONS5. At 250 rpm, the sorption mixtures were continuously stirred on a multiple magnetic stirrer. Following the sorbents' interaction with lead ions, samples were collected by centrifugation at 4000 rpm for three minutes.

Constructing the sorption process on a large scale requires continuous system sorption tests at the laboratory scale. In fixed-bed studies, small Pyrex glass

Content courtesy of Springer Nature, terms of use apply. Rights reserved.

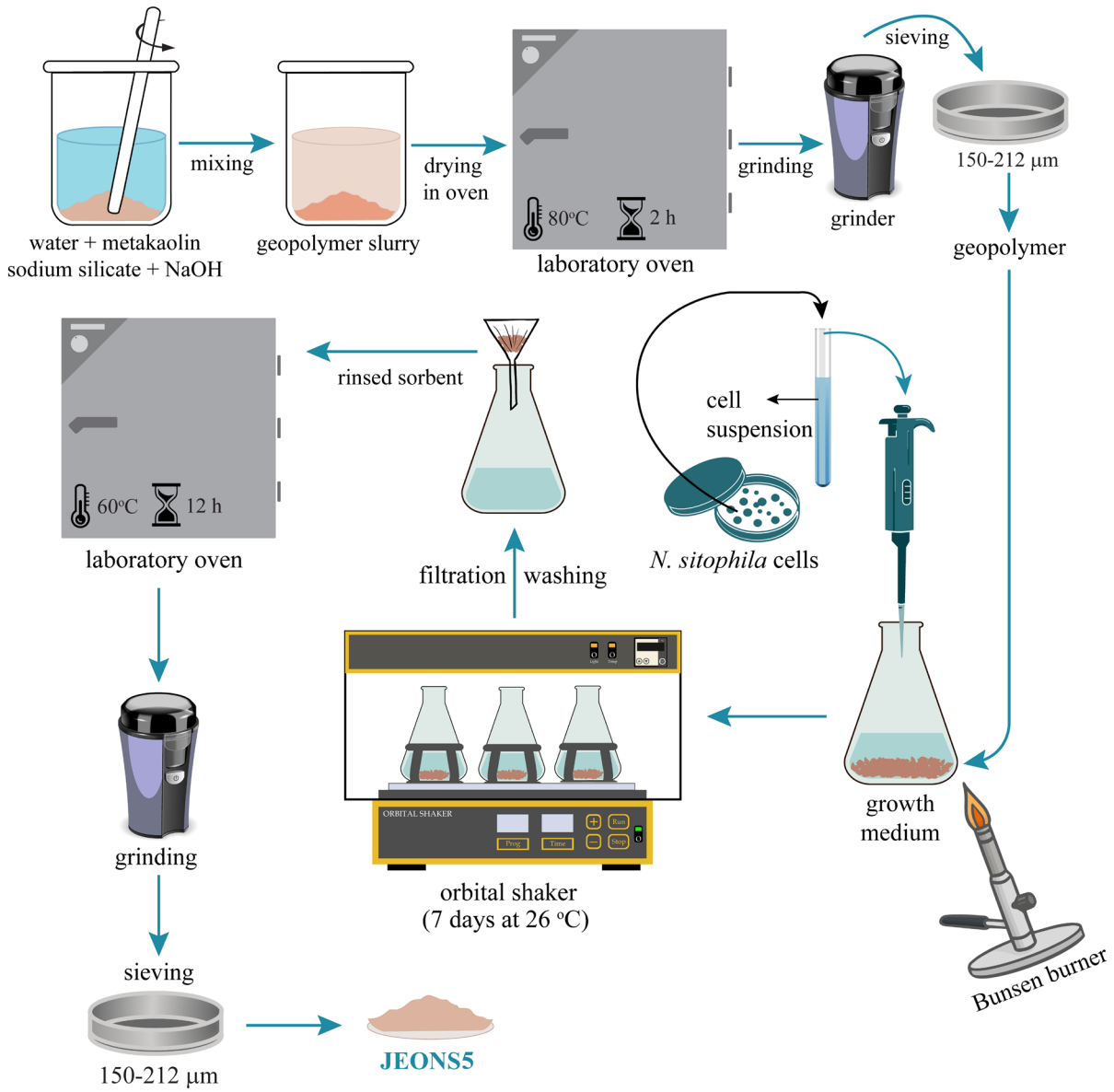

Fig. 1 The steps of the JEONS5 synthesis

columns (10.0 mm in diameter and 120.0 mm in length) were used. The sorption columns were carefully loaded with JEONS5 between two supportive sheets of glass wool to prevent any potential loss or blockage of the sorbent material during the effluent flow. Continuous mode investigations were conducted using 100 mg L^{-1} Pb^{2+} solutions. The parameters to optimize for the dynamic flow testing were the flow rate (0.5–4.0 mL min^{-1}) and the quantity of JEONS5 (0.01–0.14 g). The columns and solutions were connected using Tygon tubing. The solutions (pH 5.0) were continuously pumped through the columns using an Ismatec IP 8 peristaltic pump. Moreover, larger volumes of Pb^{2+} solutions were run through columns packed with JEONS5 to determine the breakthrough and exhaustion points of the columns and to obtain insight into the suitability of column system conditions for industrial-scale and modeling purposes.

A Perkin-Elmer AA Analyst 400 atomic absorption spectrophotometer was used to measure the

Content courtesy of Springer Nature, terms of use apply. Rights reserved.

solution's initial and final lead concentrations following centrifugation or column operations. Each experiment was conducted using three independent replicates (n = 3); the results are presented as mean ± standard error (SE), and the error bars were provided in the figures. SPSS 15.0 was used to perform statistical analysis of the data. Statistical differences between experimental groups were evaluated by one-way analysis of variance (ANOVA) test followed by Tukey's post-hoc test. Differences were considered statistically significant at $p < 0.05$. The goodness of fit of the kinetic and isotherm models was assessed using the coefficient of determination (r^2), chi-square (χ^2), *F*-value, and SE.

The values of sorption capacity (q_e) and metal removal percentage (R%) were computed using Eqs. (1), (2):

$$q_e = \frac{V(C_i - C_e)}{m} \quad (1)$$

$$\mathrm{R\%} = \frac{(C_i - C_e)}{C_i} \times 100 \quad (2)$$

The JEONS5's mass (g) is represented by m, V represents solution volume (L), and C_i and C_e denote the initial and equilibrium lead ion concentrations (mg L^{-1}), respectively.

Regeneration and real application studies

The regeneration capability of Pb^{2+}–loaded JEONS5 and its reuse potential in subsequent sorption–desorption cycles were assessed under dynamic flow conditions. In this context, Pb^{2+}–loaded columns under optimized conditions were treated with a 0.1 M EDTA solution as the eluent. Deionized water was run through the columns following the desorption process, and the cleaned columns were reconditioned for the subsequent sorption procedure. Metal sorption and desorption tests were carried out for a total of twenty cycles. The ratio of the amount of lead ions desorbed to the amount initially sorbed was used to calculate JEONS5's desorption efficiency.

Characterization experiments

In order to better understand the sorbent material's chemical characteristics and potential sorbent-sorbate interaction, a variety of analytical techniques were employed.

Fourier Transform Infrared (FTIR) spectroscopy was used to identify the functional groups on the surface. A PerkinElmer Spectrum Two (PerkinElmer, U.S.A.) spectrophotometer was used to record spectra in the 400–4000 cm^{-1} range after KBr pellet discs were prepared. An Energy-Dispersive X-ray (EDX)-equipped field emission scanning electron microscope (FESEM, Hitachi Regulus, Japan) was used to examine the surface morphology and elemental composition of the sorbent. pH-dependent zeta potential values of the sorbent material were measured using a Zeta-Meter (Malvern Zetasizer). The zeta-potential measurements were performed at pH 1, 2, 3, 4, 5, and 6, corresponding to the pH range investigated in the Pb^{2+} sorption experiments. The number of measurements at each pH was five. To conduct these measurements, JEONS5 was dispersed in ultrapure water (18.2 MΩ·cm) at a solid concentration of 1.6 g L^{-1}. The suspensions were contacted for 30 min, and the zeta potential was measured after 3 s of equilibration.

Samples were analyzed using X-ray photoelectron spectroscopy (XPS) with an Al Kα X-ray of 1486.6 eV monochromatic radiation source and a Specs-Flex apparatus (Germany). X-ray diffraction technique (XRD, Rigaku MiniFlex 600) was used to determine the crystal phase structure using monochromatic Cu Kα radiation (λ = 1.5406 Å) over a 2θ range of 5–50° at a scanning rate of 6° min^{-1}. Analyses of the samples' elemental composition were also conducted using X-ray fluorescence (XRF) spectrometry (Panalytical/Axios MAX). BET surface area measurements of the sorbent materials were carried out using Autosorb-1 (Quantachrome Instruments) in a nitrogen atmosphere.

Sorption modeling

The collected equilibrium data for the lead ion uptake process were modeled using non-linear Lagergren pseudo-first-order (PFO), pseudo-second-order (PSO), and Elovich kinetic models. The Supplementary file (Table S1 Eqs. (S1-S3)) contains formulas for these models. The equilibrium sorption behavior of Pb^{2+} on JEONS5 was investigated using the non-linear Langmuir, Freundlich, and D-R isotherm models. The Supplementary file (Table S2, Eqs. (S4–S8)) provides the formulas and parameters for

Content courtesy of Springer Nature, terms of use apply. Rights reserved.

each isotherm. The data obtained from dynamic flow mode treatment experiments were modeled using Chu's simplistic equation (Chu, 2020) (Table S3 (Eq. S14) and Table S4).

Results and discussion

Effect of sorbent dose and pH on the Pb^{2+} sorption process

In order to optimize sorbent dose and assess the proposed procedure's economic viability, it is generally acknowledged that the amount of sorbent material to be utilized in sorption is a key variable (Gado et al., 2025). The variation in Pb^{2+} sorption yields onto geopolymer and JEONS5 as a function of sorbent dose is given in Fig. 2a. This figure shows that the sorption efficiency at the lowest JEONS5 dose (0.01 g) was 58.30 ± 0.28%. As the JEONS5 dose increased, sorption efficiency increased nearly linearly, plateauing at 95.45 ± 0.06% at 0.04 g ($p > 0.05$). It is observed that the sorption efficiency of the geopolymer remains lower than that of JEONS5 at all sorbent amounts. The removal efficiency of 58.13 ± 0.68% increased up to 82.19 ± 0.58% as geopolymer mass increased from 0.04 to 0.08 g ($p < 0.05$). These results indicate that the immobilization procedure is quite effective for Pb^{2+} sorption.

At low doses of JEONS5, the binding sites of the sorbent are limited and can be saturated by the metal ions, resulting in incomplete adsorption. As the dose increases, more sites are introduced, capturing a greater fraction of metal until essentially all ions can find a site (in the high-dose limit; removal would approach 100% asymptotically). The plateau occurs when nearly all metal ions are already adsorbed, and the system is metal-limited rather than site-limited (Gado et al., 2025). In order to increase Pb^{2+} uptake while lowering the amount of JEONS5 required, a dose of 0.04 g was selected, and additional experiments were conducted using this sorbent dose. The results of (Chen et al., 2026) and (Hong et al., 2026) seem to be the same as this profile. Because of its high affinity for lead ions, JEONS5 can achieve a removal rate of over 95% even when employed at the selected sorbent dose. Good uptake behavior of the suggested sorbent material, even at relatively low doses, is an advantage that could further minimize costs, because a lower amount is required in real application situations (Ungureanu et al., 2024).

The initial pH of the solution has a significant impact on the chemistry of the metal in solution, the sorbent's surface charge, and its ionization state during sorption processes. The effect of pH values between 2.0 and 5.0 on the sorption of lead ions was investigated, as illustrated in Fig. 2b. The JEONS5's larger negative surface charge at higher pH values could potentially be a cause of the enhanced Pb^{2+} removal at pH 5.0. Additionally, there is an abundance of H^+ at highly acidic pH conditions, which may cause Pb^{2+} to compete with it for the active sites and result in zero or less Pb^{2+} uptake. The deprotonation of functional groups on the sorbent surface can account for the enhanced sorption tendency with rising pH. It means the appearance of negative areas on the sorbent surface that have the potential to interact with the metal ions. Because of the increased concentration of OH− ions in the biosorption medium, Pb^{2+} ion precipitation starts when the solution's initial pH is raised above 5.5 (Akar et al., 2024), which can also be seen from the speciation diagram of Pb species (Fig. 3). Therefore, the tests were conducted at a safe pH of 5.0, which we found to be optimum for our investigation. The pH-associated Pb^{2+} sorption pattern of JEONS5 is in line with earlier reports (Hammo et al., 2021; Kumar et al., 2023; Sayin et al., 2021; Wang et al., 2025). Furthermore, the point of zero charge pH (pH_{PZC}) of JEONS5 is approximately 2.0 (Fig. 2b), allowing it to explain the variation in Pb^{2+} removal performance at various initial pH values of the solution. At pH values below pH_{PZC}, the JEONS5 surface becomes positively charged (protonated); beyond this value, the surface gains a negative charge. Protonation and the competitive interaction between H^+ and Pb^{2+} ions cause electrostatic repulsion of positively charged surface regions at low pH, which decreases the removal efficiency of Pb^{2+}. Alongside the rise in pH, the deprotonation-induced increase in negative charge validates the enhanced sorption tendency.

Temperature effect on the Pb^{2+} sorption process

The effects of external temperature on Pb^{2+} ion sorption onto JEONS5 were investigated by experiments conducted at 15, 25, and 35 °C. Figure 2c shows that raising the temperature from 15 to 35 °C had no

Content courtesy of Springer Nature, terms of use apply. Rights reserved.

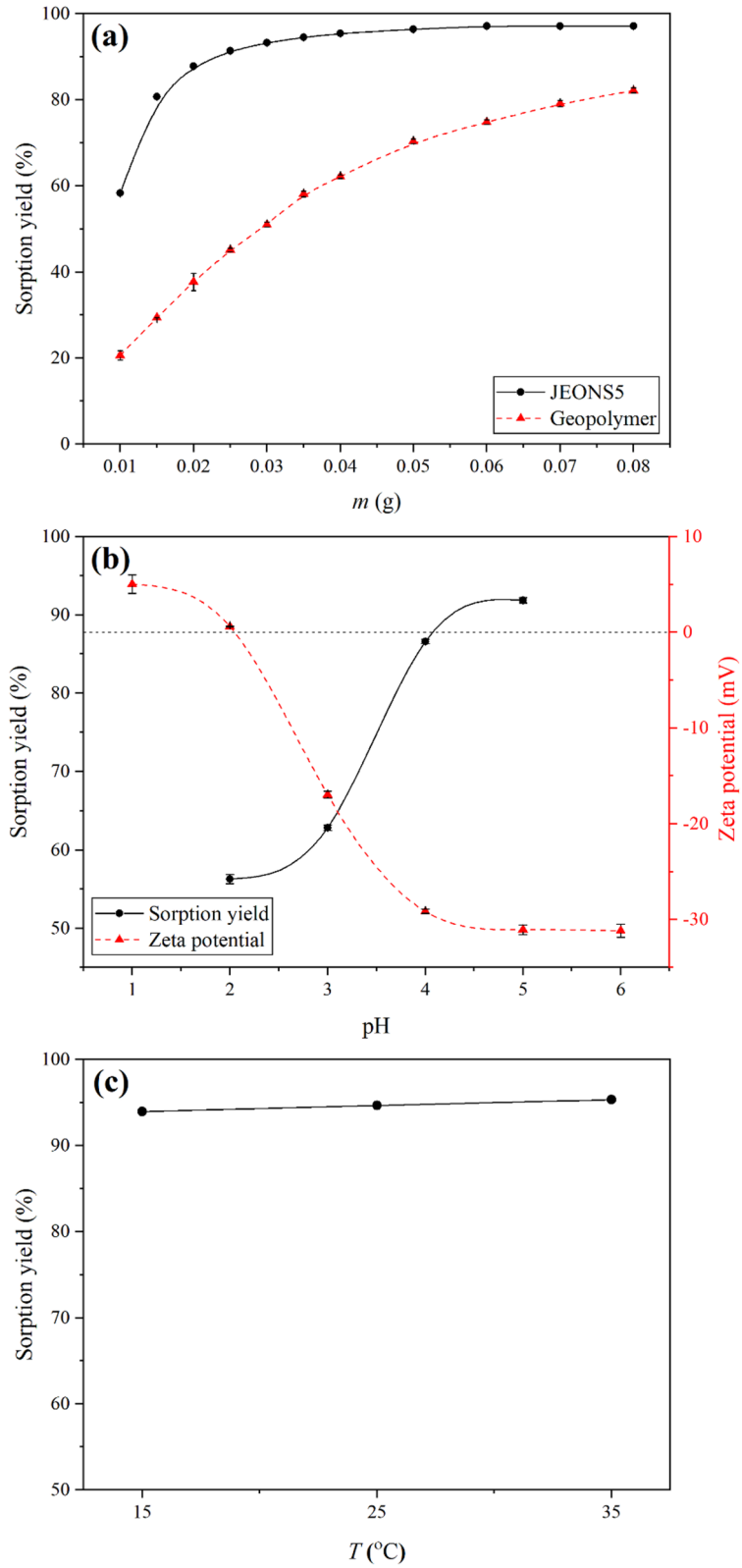

Fig. 2 Effect of sorbent amount on the Pb^{2+} sorption (**a**). Effect of pH on the Pb^{2+} sorption and zeta potential of JEONS5 (**b**). Effect of temperature on the Pb^{2+} sorption (**c**)

Content courtesy of Springer Nature, terms of use apply. Rights reserved.

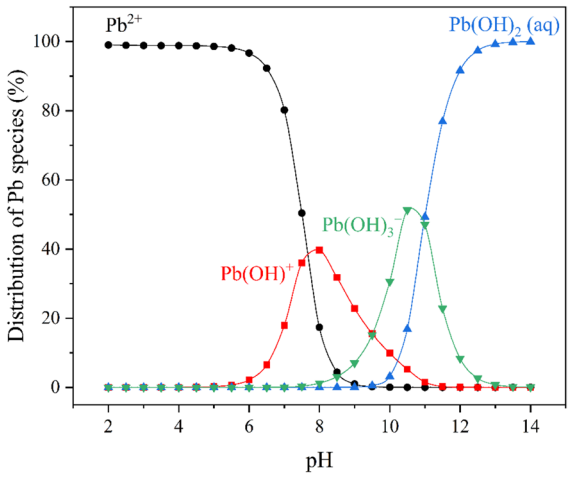

Fig. 3 Pb^{2+} speciation in aqueous solution determined using MINTEQ 4.0 software (T: 25 °C, Pb^{2+} concentration: 100 mg L^{-1})

discernible effect on the Pb^{2+} adsorption efficiency of JEONS5 ($p > 0.05$). An ideal criterion for the developed sorbents to be evaluated in terms of broader applications is that the sorption process remains unaffected by temperature (Vijayaraghavan & Yun, 2008). An insignificant effect of temperature suggests that adsorption is only weakly temperature-dependent within the investigated temperature range. The hybrid sorbent proposed in this study has a significant advantage for use in large-scale industrial applications, as it will not require temperature adjustment.

Kinetic modeling of Pb^{2+} sorption onto JEONS5

The kinetic behavior of Pb^{2+} sorption onto JEONS5 was investigated at different contact times (Fig. 4a). Approximately 75% of the Pb^{2+} was sorbed by JEONS5 in the first five minutes, indicating that the sorption process was fast. In 30 min, equilibrium was achieved, as shown in this figure ($p > 0.05$).

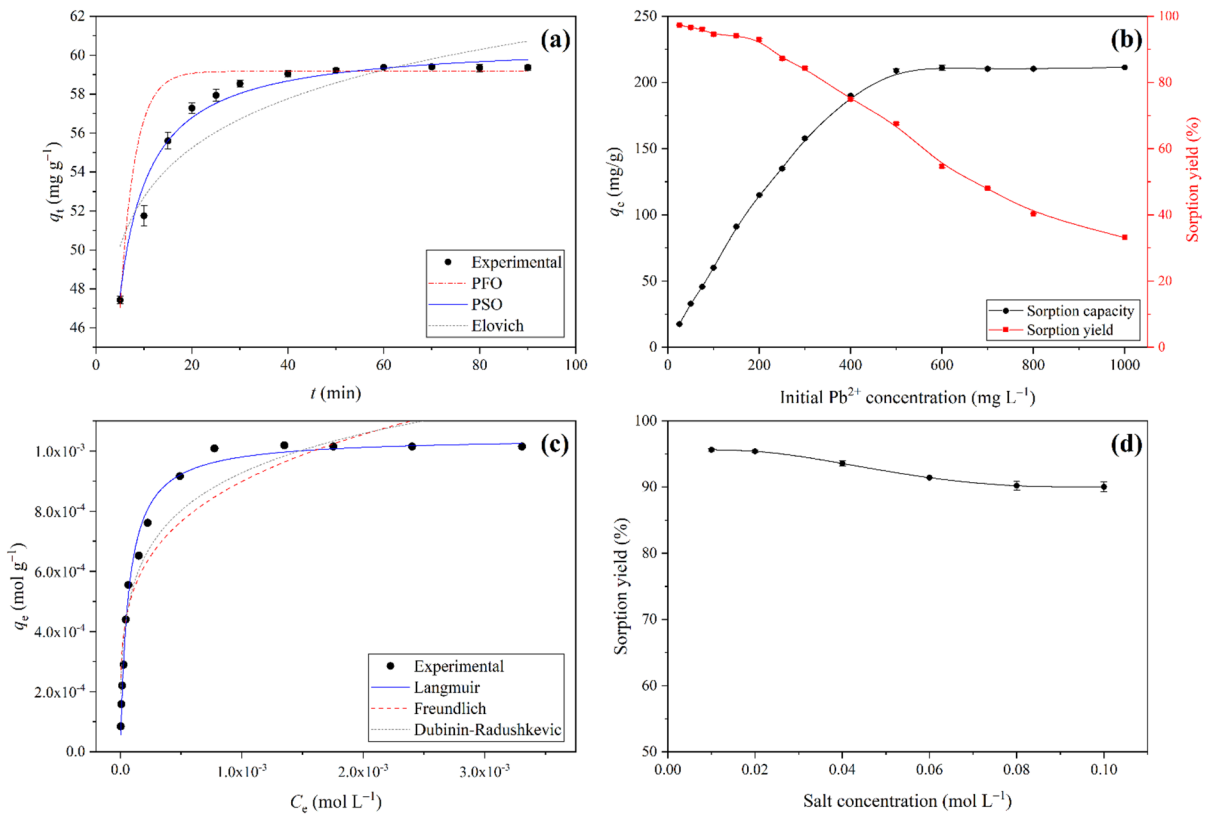

Fig. 4 Time-dependent data and kinetic plots for Pb^{2+} sorption by JEONS5 (**a**). Effect of initial sorbate concentration on the Pb^{2+} sorption (**b**). Isotherm plots for the Pb^{2+} sorption by JEONS5 (**c**). Effect of ionic strength on the Pb^{2+} sorption (**d**)

Content courtesy of Springer Nature, terms of use apply. Rights reserved.

JEONS5's rapid sorption behavior may be attributed to its suitable surface structure, as demonstrated by the SEM examination. In realistic sorption applications, rapid sorption kinetics are critical for process effectiveness and economy. JEONS5 offers a significant advantage in this context for the Pb^{2+} removal procedure.

Kinetic data modeling was used to determine the kinetic rate constant and understand the dynamic nature of sorption. The pseudo-first order (Lagergren, 1898), pseudo-second order (Ho & McKay, 1999), and Elovich (Zeldowitsch, 1934) kinetic models provided by the equations (Equations (S1)–(S3)) in Table S1 (Supplementary Materials) were used to evaluate the uptake of Pb^{2+} by JEONS5. The models' non-linear fits are displayed in Fig. 4a, and the kinetic parameters are compiled in Table 1. Evaluation of the model parameters (R^2 ~ 1, low χ^2, and high F) indicates that the sorption kinetics are better described by the PSO model. In addition, the experimentally determined sorption capacity (58.54 ± 0.17 mg g^{-1}) agreed well with the calculated sorption capacity obtained from the PSO model (60.69 ± 0.12 mg g^{-1}). These findings suggest that chemisorption may play a major role in the sorption process (Zhang et al., 2023b). Nevertheless, the model by itself does not offer conclusive proof of the sorption mechanism. Similar kinetic results were previously found in Pb^{2+} sorption on goethite-modified and unmodified *Albizia lebbeck* (Alabi et al., 2026) and sodium alginate-lotus carbon dots composite adsorbent (Younis et al., 2025).

Effect of initial Pb^{2+} concentration on the sorption process and isotherm modeling

The Pb^{2+} sorption performance of JEONS5 was investigated at different initial Pb^{2+} concentrations ranging from 25 to 1000 mg L^{-1} (Fig. 4b). As the initial Pb^{2+} ion concentration was increased from 25 to 500 mg L^{-1}, the sorption capacity of JEONS5 rapidly increased from 17.63 ± 0.02 to 208.95±1.26 mg g^{-1} ($p < 0.05$). No significant difference in the sorption capacity of JEONS5 was observed at higher initial Pb^{2+} concentrations, indicating that the sorbent material has reached a saturation point ($p > 0.05$). On the other hand, the sorption yield of JEONS5 decreased from 97.30 ± 0.21% to 67.52 ± 0.38% when the initial Pb^{2+} concentration increased from 25 to 500 mg L^{-1} ($p < 0.05$).

Identifying the maximal sorption capacity of a particular sorbent requires knowledge of the isotherm data acquired under sorption equilibrium conditions. Because they provide information on how the sorbent interacts with the sorbate at different concentrations, these data are also essential for developing an efficient sorption process. This allows the sorption settings to be optimized for maximum efficiency.

The sorption behavior of JEONS5 was assessed using the Langmuir, Freundlich, and Dubinin Radushevich (D-R) isotherm models. The Supplementary file contains the formulas for the Langmuir, Freundlich, and D-R isotherms (Table S2, Equations (S4-S8)). According to the Langmuir model, sorbates bind to sorption sites through monolayer sorption, in which there are no interactions between the molecules/ions of the sorbate. Instead of single-layer coverage, the Freundlich isotherm model relies on the multilayer sorption of contaminating molecules or ions. On the other hand, the D-R isotherm model and the mean energy of sorption can be used to assess the physical or chemical characteristics of sorption processes (Dubinin & Radushkevich, 1947). The Langmuir model could more accurately represent the sorption of Pb^{2+} by JEONS5, according to the coefficient of determination values obtained from fitting of these isotherms (Fig. 4c). The better fit of the Langmuir model over the Freundlich and D-R models implies that the sorption process is mainly represented by monolayer coating in the most energetically favorable sorption regions, despite the structurally heterogeneous properties of the proposed sorbent JEONS5. Consequently, the Langmuir fit should be interpreted as a representation of the predominant sorption behavior under the conditions under study rather than as direct proof of an entirely homogeneous sorbent surface. The predicted maximal Pb^{2+} uptake quantity of JEONS5 was 1.05×10^{-3} mol g^{-1} (217.56 ± 3.53 mg g^{-1}) (Table 1), which is consistent with the experimental measurement of 1.02×10^{-3} mol g^{-1} (211.15 ± 1.80 mg g^{-1}).

Table S5 compares the maximal Pb^{2+} removal capacity of JEONS5 with the capabilities of a few other immobilized sorbents found in the literature. Direct quantitative ranking is not strictly appropriate because sorption capacities are strongly influenced by experimental parameters such as initial metal

Content courtesy of Springer Nature, terms of use apply. Rights reserved.

Table 1 Kinetic and isotherm parameters for the sorption of Pb^{2+} onto JEONS5

Kinetic models							
Model	Value	SE	Value	SE	χ^2	F	r^2
PFO	q_e (mg g^{-1})		k_1 (min^{-1})		23.49	4.66×10^4	0.939
	59.17	(±0.20)	0.317	(±0.016)			
PSO	q_e (mg g^{-1})		k_2 (g mg^{-1} min^{-1})		4.89	2.24×10^5	0.987
	60.69	(±0.12)	0.012	(±0.006)			
Elovich	α (mg g^{-1} min^{-1})		β (g mg^{-1})		70.77	4.45×10^1	0.816
	7.02×10^5	($\pm15.9\times10^5$)	0.27	(±0.04)			
Isotherm models							
Model	Value	SE	Value	SE	χ^2	F	r^2
Langmuir	q_m (mol g^{-1})		K_L (L mol^{-1})		1.25×10^{-9}	3.05×10^3	0.991
	1.05×10^{-3}	($\pm0.02\times10^{-3}$)	1.49×10^4	($\pm0.12\times10^4$)			
Freundlich	n		K_F ((mol g^{-1}) (L $mol^{-1})^{1/n}$)		1.54×10^{-8}	2.42×10^2	0.892
	4.30	(±0.56)	4.49×10^{-3}	($\pm0.96\times10^{-3}$)			
D–R	q_m (mol g^{-1})		E (kJ mol^{-1})		9.11×10^{-9}	4.14×10^2	0.937
	1.86×10^{-3}	($\pm0.16\times10^{-3}$)	14.98				

*SE: standard error of the mean, *χ^2: chi-square, F: F-statistic, r^2: coefficient of determination

Content courtesy of Springer Nature, terms of use apply. Rights reserved.

concentration, solution pH, sorbent dosage, contact time, temperature, etc., even though the observed Pb^{2+} sorption capacity falls within the range of high-performing sorbents. In conclusion, rather than being a final ranking of sorbent efficiency, this comparison could be considered an overall performance evaluation.

Ionic strength impact on the Pb^{2+} sorption

The effect of ionic strength on Pb^{2+} sorption with JEONS5 was investigated under optimum conditions with sorption mixtures containing KNO_3 at different concentrations. The results are given in Fig. 4d. Accordingly, the addition of KNO_3 with a concentration ranging from 0.01 to 0.1 mol L^{-1} caused a slight decrease in Pb^{2+} sorption efficiency from 95.63 ± 0.22 to $90.05 \pm 0.74\%$ ($p < 0.05$). Depending on their affinity, ionic species in the medium could compete with metal ions for binding to the limited active sites on the sorbent surface. The sorption efficacy of the sorbent material may be decreased in this case. Ionic strength can also affect particle aggregation by altering electrostatic interactions and can restrict the transfer of metal ions from the solution to the sorbent surface by affecting the activity coefficient of metal ions (Tan et al., 2015). Similar sorption patterns have been reported in the literature regarding the influence of ionic strength on sorption (Çelik et al., 2017; Low et al., 2000).

Dynamic flow sorption by JEONS5 and breakthrough curve

Dynamic-flow mode sorption studies at the laboratory scale are crucial for the planning and forecasting of large-scale sorption treatment processes. Here, the flow rate and the quantity of sorbent packed into columns are important factors that have a direct bearing on treatment effectiveness in sorption column applications. Additionally, understanding the dynamic responsiveness and mode of operation of the adsorption column depends on the breakthrough curve (Akar et al., 2024).

Flow rates at 0.5, 1.0, 2.0, 3.0, and 4.0 mL min^{-1} were investigated to examine the effect of flow rate on Pb^{2+} uptake by JEONS5. The findings are shown in Fig. 5a. JEONS5 had the highest Pb^{2+} removal efficacy at flow rates of 0.5 and 1.0 mL min^{-1}. $98.54 \pm 0.33\%$ (25.38 ± 0.08 mg g^{-1}) was the Pb^{2+} sorption efficiency of JEONS5 at a flow rate of 1 mL min^{-1}; however, the sorption efficiency decreased by 10.12% ($p < 0.05$) as the flow rate was raised from 1.0 to 4.0 mL min^{-1}.

The reduced metal uptake yield at higher flow rates could be due to the solution's diffusion restrictions into the sorbent structure's pores and the insufficient contact time between the solute and the JEONS5 loaded in the column. Metal ions have greater time to interact with JEONS5 binding sites at lower flow rates, increasing the yields of metal sorption. This led to the conclusion that 1.0 mL min^{-1} was the optimal flow rate for subsequent continuous system operations. The identical findings were noticed in earlier studies that used *Vetiveria zizanioides* biochar (Tyagi, 2022) and silica gel-coated *Lactarius* biomass (Akar et al., 2013b) to treat metal-laden solutions.

Figure 5b displays the findings of an investigation into the impact of loading JEONS5 into columns in amounts ranging from 0.01 to 0.14 g on the efficient removal of Pb^{2+} ions with an optimum flow rate of 1.0 mL min^{-1}. By increasing the amount from 0.01 to 0.1 g, JEONS5's dynamic flow mode sorption performance showed a substantial improvement ($p < 0.05$), achieving a removal efficiency of $98.15 \pm 0.08\%$ (25.57 ± 0.02 mg g^{-1}). After this, the hybrid sorbent's binding sites were saturated ($p > 0.05$), which prevented a substantial change in the metal sorption yield. The outcomes of the batch processing approach also showed a similar trend. The observed increase in sorption efficiency can be attributed to an increase in bed height in the column as the amount of sorbent increases (Suter et al., 2025). Higher bed height is linked to more sorbent binding sites for heavy metal uptake when flow rate and initial metal ion concentration are constant. This enables sorbent materials to interact with target heavy metal ions for longer periods of time, resulting in increased water purification in the continuous system (Olatunji et al., 2024). In other words, JEONS5 may have uptake more Pb^{2+} ions due to the extended mass transfer zone in the column. Studies in the literature that used various amounts of sorbent in column systems have reported similar outcomes (Akar et al., 2013a; Pakshirajan & Swaminathan, 2006).

Utilizing the specified optimal dynamic flow conditions (*m*: 0.1 g, flow rate: 1.0 mL min^{-1}, bed height: 4 mm, empty bed contact time: 0.35 min),

Content courtesy of Springer Nature, terms of use apply. Rights reserved.

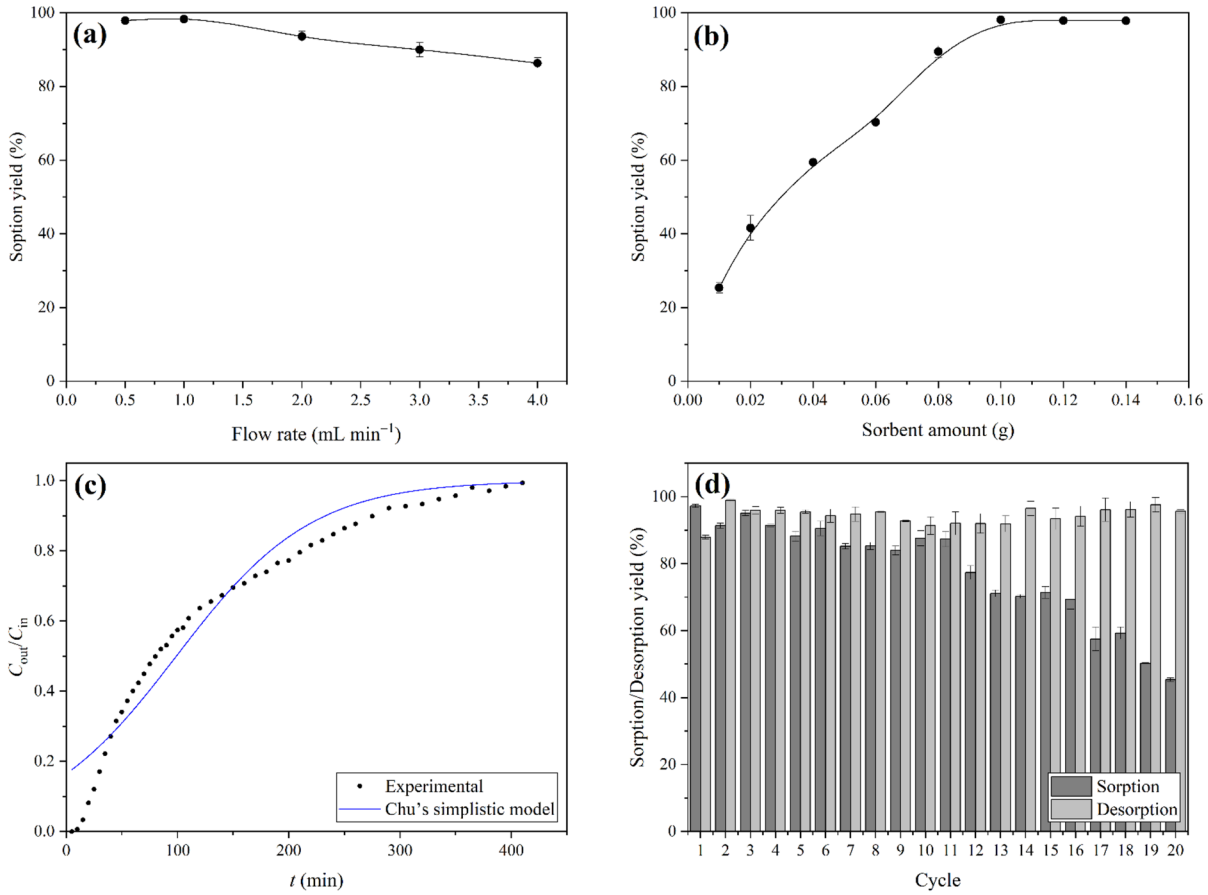

Fig. 5 **a.** Effect of flow rate on the Pb^{2+} sorption in a continuous system. **b.** Effect of sorbent dosage on the Pb^{2+} sorption in a continuous system. **c.** Breakthrough curve for Pb^{2+} sorption onto JEONS5. **d.** Sorption and desorption cycles for Pb^{2+} removal in a continuous system

the breakthrough curve for JEONS5 was generated and shown in Fig. 5c. Experimental breakthrough (C_{out}/C_{in}=0.05) and exhaustion (C_{out}/C_{in}=0.95) times were found to be 20 and 350 min, respectively. The column's sorption parameters were determined using Eq. S9–S13 (Supplementary file) (Aksu & Gönen, 2004). In breakthrough curve modeling, the Bohart-Adams (B–A), Thomas, and Yoon-Nelson (Y–N) models are frequently employed in dynamic examinations. Nevertheless, Chu demonstrates that these models are mathematically identical and analogous through the simplified equation (Chu, 2020) (Table S3, Eq. S14, Supplementary file). The related model parameters (a and b) used for calculation of B–A, Thomas, and Y–N coefficients are listed in Table S4 (Supplementary file).

The parameters that were derived from this simplified equation can be observed in Table 2. This model exhibits very good agreement with the data from the experiments, as indicated by the level of correlation

Table 2 Continuous sorption efficiency and breakthrough curve parameters

V_{eff} (mL)	q_b (mg g^{-1})	q_e (mg g^{-1})	m_{ad} (mg)	R% (%)	Z_m (mm)	k_{BA}. k_T (mL mg^{-1} min^{-1})	N_o (mg L^{-1})	q_T (mg g^{-1})	k_{YN} (min^{-1})	τ (min)	r^2
350	19.37	114.98	11.50	32.37	3.77	0.162	11.54	100.33	0.0297	98.8	0.943

Content courtesy of Springer Nature, terms of use apply. Rights reserved.

(r^2 = 0.943). The dynamic uptake capacity from the Thomas model (q_T = 100.33 mg g^{-1}) and the experimental value (q_e = 114.98 mg g^{-1}) show that JEONS5 can be used successfully in a sorption column system. The sorption performance of Pb^{2+} at the 50% breakpoint (τ) also agrees well with experimental data (85 min). The findings indicated that JEONS5 may be used in a fixed-bed sorptive treatment method to effectively eliminate Pb^{2+} from water-based environments.

Table S6 shows the dynamic sorption capacities of Pb^{2+} for several sorbents that have been described previously in publications. JEONS5 seems to show a high sorption capacity under dynamic-flow conditions. It should be noted that the settings and system configurations in the aforementioned studies varied.

Regeneration ability and real sample application of JEONS5

Because the exhausted sorbent laden with heavy metal ions is an unsafe material that pollutes the environment, disposing of it could lead to additional environmental issues. Using one of the elimination techniques (such as pyrolysis, incineration, or elution) may help address this issue. The most popular method in this context is elution, which enables the recovery of heavy metal ion solutions at higher concentrations for inertization and the reuse of the adsorbent for later applications. From an economic point of view, sorbent material regeneration is critical (Han et al., 2009).

JEONS5's sorption and desorption properties were evaluated using 20 successive sorption and desorption cycles. Both sorption and desorption efficiencies were approximately 90% until the end of the 11th cycle. However, in the subsequent cycles, a decline in the sorption efficiencies was noted, and in the 20th cycle, a sorption efficiency of approximately 50% was achieved, despite high desorption efficiencies (greater than 90%) (Fig. 5d). These results demonstrated the high sorption/desorption performance of JEONS5 through 10 consecutive cycles, which also suggests that it has good reusability potential. JEONS5 exhibits a desorption potential of over 90% even after 20 cycles, making it a useful sorbent for practical applications. The decrease in the sorption efficiency of JEONS5 in subsequent cycles may be attributed to interactions between the complexing agent and the sorbent's functional groups or active sites. These sites are thought to be permanently occupied and blocked by metal that was adsorbed in the preceding cycle (Hammaini et al., 2007).

Using real wastewater samples, JEONS5's Pb^{2+} removal efficiency was evaluated in batch and column systems to gauge the sorbent's performance under practical conditions. The wastewater samples, whose contents are listed in Table S7. The real wastewater samples were collected from a metal processing facility in the Turkish province of Eskişehir and a textile manufacturing plant in the province of Bursa in June 2025 and transported to the laboratory in high-density polyethylene (HDPE) bottles. The suspended solids were removed by vacuum filtration through filter paper, and samples were stored at 4 ℃ in a refrigerator. The storage period before the sorption experiments was 7 days. The initial pH of the metal processing and textile manufacturing wastewater was 5.7 and 6.8, respectively. Competing-ion concentrations were not measured after sorption experiments. Under optimized conditions for both systems, spiked wastewater (100 mg L^{-1} Pb^{2+}) was used in these practical investigations. The sorption efficiency of JEONS5 for Pb^{2+} removal was 90.54 ± 0.22% and 95.55 ± 0.07% in metal processing wastewater under batch and continuous systems, respectively. Likewise, for the removal of Pb^{2+} from textile industry effluent, sorption efficiencies of 92.19 ± 0.34% and 96.07 ± 0.14% were obtained in the batch and continuous systems, respectively. The findings demonstrated that, under the experimental conditions investigated, the sorbent material successfully eliminated Pb^{2+} ions from real wastewater samples. However, these results should not be taken as conclusive evidence that matrix effects do not exist because actual wastewater can be complicated and variable. Subject to additional validation under a broader range of operating circumstances, the results suggest that JEONS5 is a promising material for Pb^{2+} removal from wastewater and may have potential for practical wastewater treatment applications.

Characteristic features of JEONS5

SEM images and EDX micrographs of the geopolymer, JEONS5, and Pb^{2+}-loaded JEONS5 are shown in Fig. 6. The geopolymer support has a dense, rough, and porous surface morphology, indicating a heterogeneous surface structure. The EDX spectrum of the

Content courtesy of Springer Nature, terms of use apply. Rights reserved.

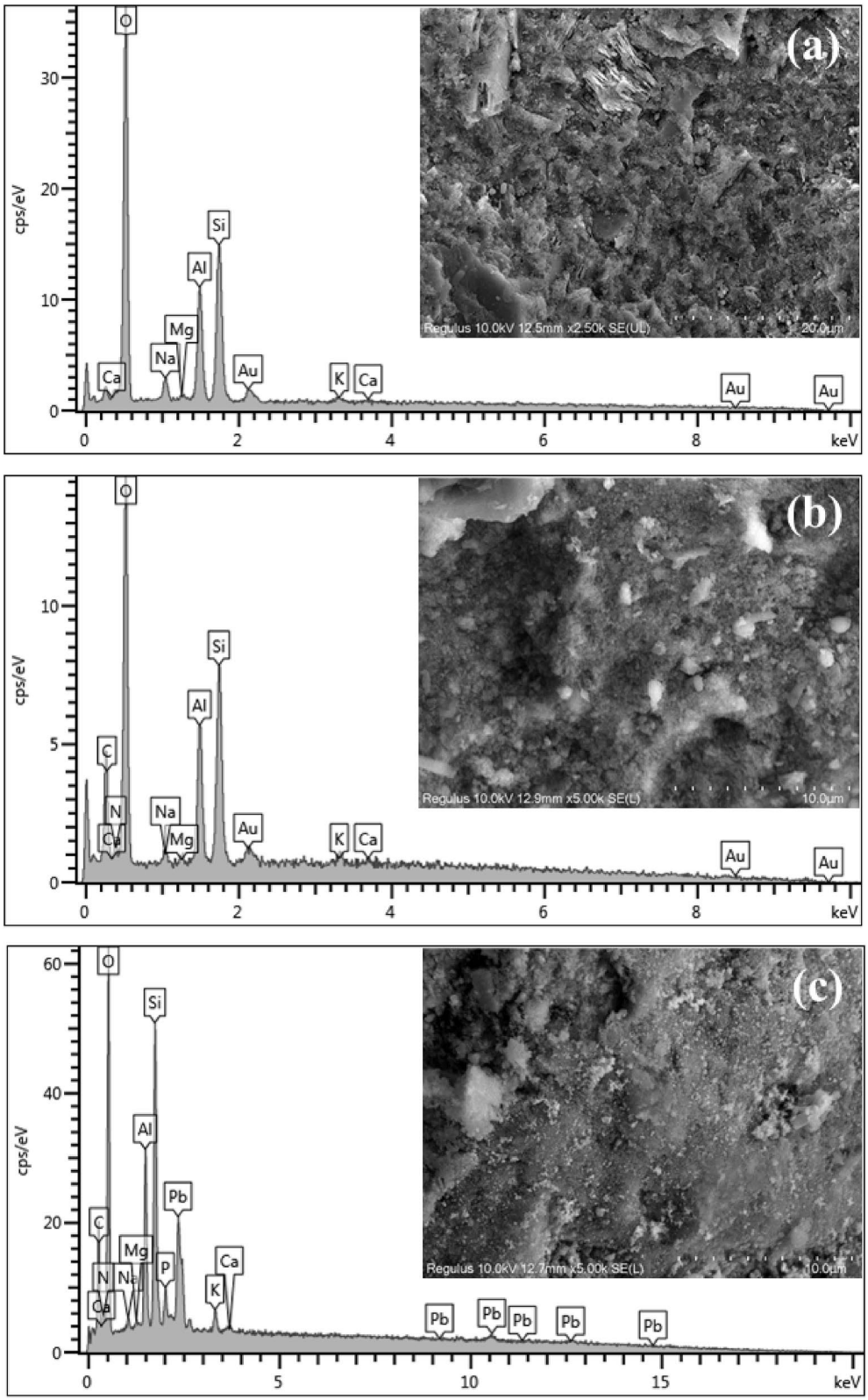

Content courtesy of Springer Nature, terms of use apply. Rights reserved.

◂**Fig. 6** EDX spectra and SEM micrographs of geopolymer (**a**), JEONS5 (**b**), and Pb^{2+}-loaded JEONS5 (**c**)

geopolymer reveals the predominant elements Si, Al, O, and Na, with trace quantities of Ca and K, as expected (Fig. 6a). A coarse and rougher structure with an unidentified geometry and a spongy surface is likely seen in the JEONS5 SEM micrograph. The hybrid sorbent is mostly composed of carbon (C), silicon (Si), oxygen (O), and aluminum (Al), with trace amounts of magnesium (Mg), sodium (Na), and potassium (K), according to the EDX analysis in Fig. 6b. The reduction of the percentages of Si, Al, and Na was observed in addition to the identification of carbon (C), which is absent in the spectrum of the geopolymer structure in the spectrum of JEONS5. These results provide proof of the immobilization process. In addition to the pre-existing peaks, the Pb^{2+} signal, which was not visible in the hybrid sorbent spectrum before sorption, became evident following the sorption process (Fig. 6c). This finding convincingly shows that Pb^{2+} ions were sorbed onto JEONS5 and is in line with the SEM image, which displays a comparatively fuller and smoother surface and particulate structures in the form of small aggregates following sorption. Furthermore, Na, K, and Ca amounts are reduced, which may show that ion exchange is one of the most efficient mechanisms.

FTIR spectra of the geopolymer, JEONS5, and Pb^{2+}-loaded JEONS5 are shown in Fig. 7a. Particularly noteworthy are the broad peak at 3440 cm^{-1} originating from –OH groups, the relatively intense peak at 1647 cm^{-1}, the peak observed at approximately 1403 cm^{-1} that can be attributed to the formation of Na_2CO_3 on the geopolymer surface, the sharp peak at 1031 cm^{-1} that can be associated with the Si–O–Si/Si–O–Al asymmetric stretching vibration, the peaks in the 500–800 cm^{-1} range, thought to be due to Al–O–Si bending vibrations, and the peak at 441 cm^{-1}, also thought to be due to Si–O–Si bending vibrations, in the FTIR spectrum of the geopolymer used as a support material in microbial immobilization (Blanco et al., 2023; Kara et al., 2018; Wei et al., 2022). In the IR spectrum of JEONS5 (Fig. 7a), a shift in the –OH/–NH band (from 3440 to 3421 cm^{-1}), an increase in the intensity of the peaks associated with the $–CH_2$ and $–CH_3$ groups (at 2979 cm^{-1} and 2934 cm^{-1}), and an increase in the intensity of the peak (1647 cm^{-1}) attributable to C−N or H−O−H groups. All these findings show that the fungal cells have been effectively immobilized within the geopolymer structure, forming a composite sorbent.

Following the Pb^{2+} sorption with JEONS5, a slight shift in the –OH/–NH band (from 3421 to 3418 cm^{-1}) was observed in the FTIR spectrum of the sorbent material (Fig. 7a). Similar shifts were noted in the peak linked to the C=O, C−N (amide I), and H−O−H groups (from 1647 to 1650 cm^{-1}), the band corresponding to Al−O−Si (from 598 to 573 cm^{-1}), and the peak associated with Si−O−Si (from 441 to 454 cm^{-1}). Additionally, a new peak observed at 1384 cm^{-1} may correspond to the asymmetric N–O stretching vibration of nitrate, resulting from the sorption of nitrate ions in the working solutions prepared from $Pb(NO_3)_2$. These changes suggest the possible interaction between JEONS5 and Pb^{2+} via the mentioned functional groups.

Examining the XRD spectrum of JEONS5 in Fig. 7b, a broad hump located between 15 and 40° 2θ indicates an amorphous structure of the sample, as expected, because both biomass and geopolymers have an amorphous structure. The two minor peaks at 20.9° and 26.7° 2θ are due to quartz, an impurity phase present in the metakaolin used to prepare the geopolymer. After Pb^{2+} sorption, the sample remains predominantly amorphous, although minor unidentified diffraction peaks appear at 21.6° and 30.1° 2θ. The retention of the broad amorphous band indicates that the overall amorphous character of JEONS5 is preserved after Pb^{2+} sorption.

The BET specific surface area, pore size distribution, and pore diameter generally provide direct or indirect information about the sorbent's sorption performance in removing contaminants, based on the active sorption sites on its surface. It was observed that the specific surface area, total pore volume, and average pore size of JEONS5 were higher than those of the fungal biomass (Table 3). A decrease in micropore volume was observed. The geopolymer used as the support material exhibited a greater surface area and pore volume compared to *N. sitophila* and JEONS5. Comparison of the three materials indicates that the geopolymer component substantially enhances the specific surface area and average pore size. Although comparisons in the literature generally focus only on specific surface areas, in many cases, the effect of larger pore size on increased sorption efficiency can be more significant than that of

Content courtesy of Springer Nature, terms of use apply. Rights reserved.

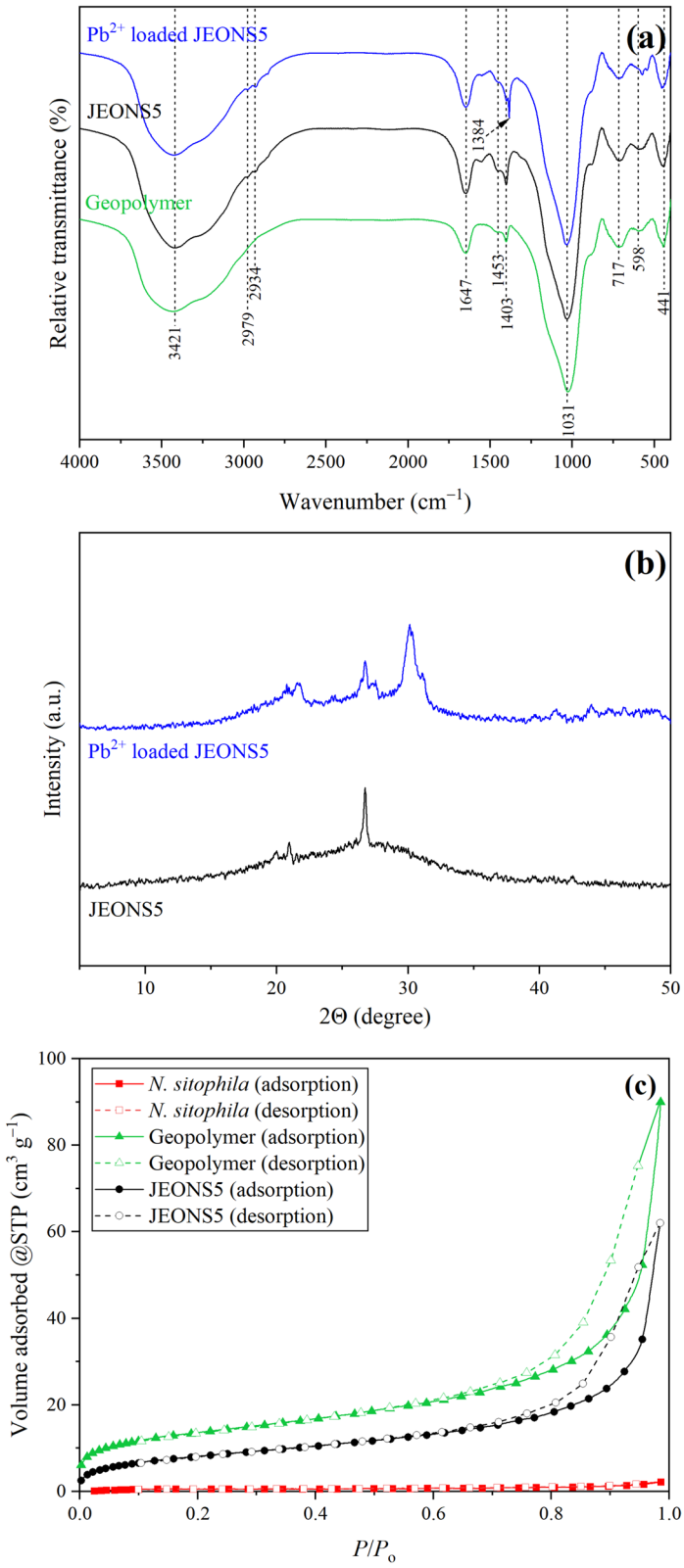

Fig. 7 FTIR spectra of geopolymer, JEONS5, and Pb^{2+}-loaded JEONS5 (**a**), XRD pattern of JEONS5 and Pb^{2+}-loaded JEONS5 (**b**), multipoint BET nitrogen adsorption–desorption isotherms of *N. sitophila*, geopolymer, and JEONS5 (**c**)

Content courtesy of Springer Nature, terms of use apply. Rights reserved.

Table 3 BET specific surface area analysis of *N. sitophila*, geopolymer, and JEONS5

		N. sitophila	Geopolymer	JEONS5
BET specific surface area	($m^2\ g^{-1}$)	4.33	49.11	29.98
Total pore volume	($mm^3\ g^{-1}$)	3.34	139.55	96.09
Micropore volume	($mm^3\ g^{-1}$)	0.66	4.58	0.10
Average pore size	(nm)	1.54	5.68	6.41

Table 4 XRF results of sorbent materials

Component		JEONS5	JEONS5-Pb^{2+}
SiO_2	(%)	35.06	33.45
Al_2O_3	(%)	17.92	17.38
Na_2O	(%)	1.60	0.86
K_2O	(%)	2.57	1.83
P_2O_5	(%)	2.42	2.22
CaO	(%)	1.32	1.20
MgO	(%)	0.89	0.69
PbO	(%)	–	9.42
TiO_2	(%)	0.25	0.26
Fe_2O_3	(%)	0.45	0.39
Cl	(%)	0.15	0.16
I	(%)	–	0.09
SO_3	(%)	0.04	0.08

specific surface area (Dou et al., 2022). In the present study, the increase in average pore size following the immobilization process may be associated with enhanced sorption efficiency. The nitrogen adsorption isotherms of NS, geopolymer, and JEONS5 (Fig. 7c) could be classified as Type IV isotherms, accompanied by adsorption–desorption hysteresis at relatively high relative pressures. This behavior is characteristic of mesoporous materials and is consistent with the average pore diameters of JEONS5 (Table 3), which fall within the mesoporous range (2–50 nm) (Lester et al., 2004).

XRF spectroscopy was used to determine the elemental composition of JEONS5 both before and after metal loading; the results are displayed in Table 4. The findings demonstrated that phosphorus pentoxide (P_2O_5), potassium oxide (K_2O), and aluminum oxide (Al_2O_3) are present in significant amounts in the structure of JEONS5, in addition to the predominance of silicon dioxide (SiO_2). Additionally, JEONS5's secondary compounds are linked to Mg, Ca, and Na.

Figure 8 displays the XPS spectra of geopolymer and JEONS5 both prior to and following the sorption process. The XPS spectrum of JEONS5 (Fig. 8b) reveals the presence of Si, O, and Al originating from the geopolymer matrix (Fig. 8a) (Lan et al., 2019; Zhang et al., 2022). In addition, minor peaks of Ca, Na, P, and K accompany the major peaks of C, O, and N, which are also reported in the literature for fungal biomass (Zhao et al., 2016). These results clearly validate the hybrid sorbent structure. The peaks that occur at 416 eV, 438 eV, and 646 eV, which are characteristic of Pb $4d_{5/2}$, Pb $4d_{3/2}$, and Pb $4p_{3/2}$, when the XPS spectra of JEONS5 following Pb^{2+} sorption (Fig. 8c) are analyzed, clearly demonstrate the sorption of Pb^{2+} to the material surface (Ding et al., 2016; Zhang et al., 2023a). This result provides additional significant proof of a successful sorption process, which is also supported by the other characterization techniques.

Sorption mechanism

To understand more about the possible mechanisms for the biosorption of Pb^{2+} onto JEONS5, physicochemical characterization techniques, biosorption data, and theoretical models were considered together. The experimental results indicate that the removal of Pb^{2+} is controlled by more than one simultaneous interaction rather than by a single mechanism. The pH-dependent sorption behavior and zeta-potential results indicate that changes in the surface charge of JEONS5 may influence Pb^{2+} uptake and suggest that electrostatic interactions contribute to the sorption process. The slight decrease in Pb^{2+} sorption efficiency as ionic strength increases is also consistent with the involvement of electrostatic interactions. However, these observations still do not definitively indicate that electrostatic interactions play a dominant role in the process. According to the PSO kinetic model assumptions, Pb^{2+} biosorption on JEONS5 may also have contributed to the removal process by chemical sorption via electron sharing or electron transfer between Pb^{2+} ions in the liquid

Content courtesy of Springer Nature, terms of use apply. Rights reserved.

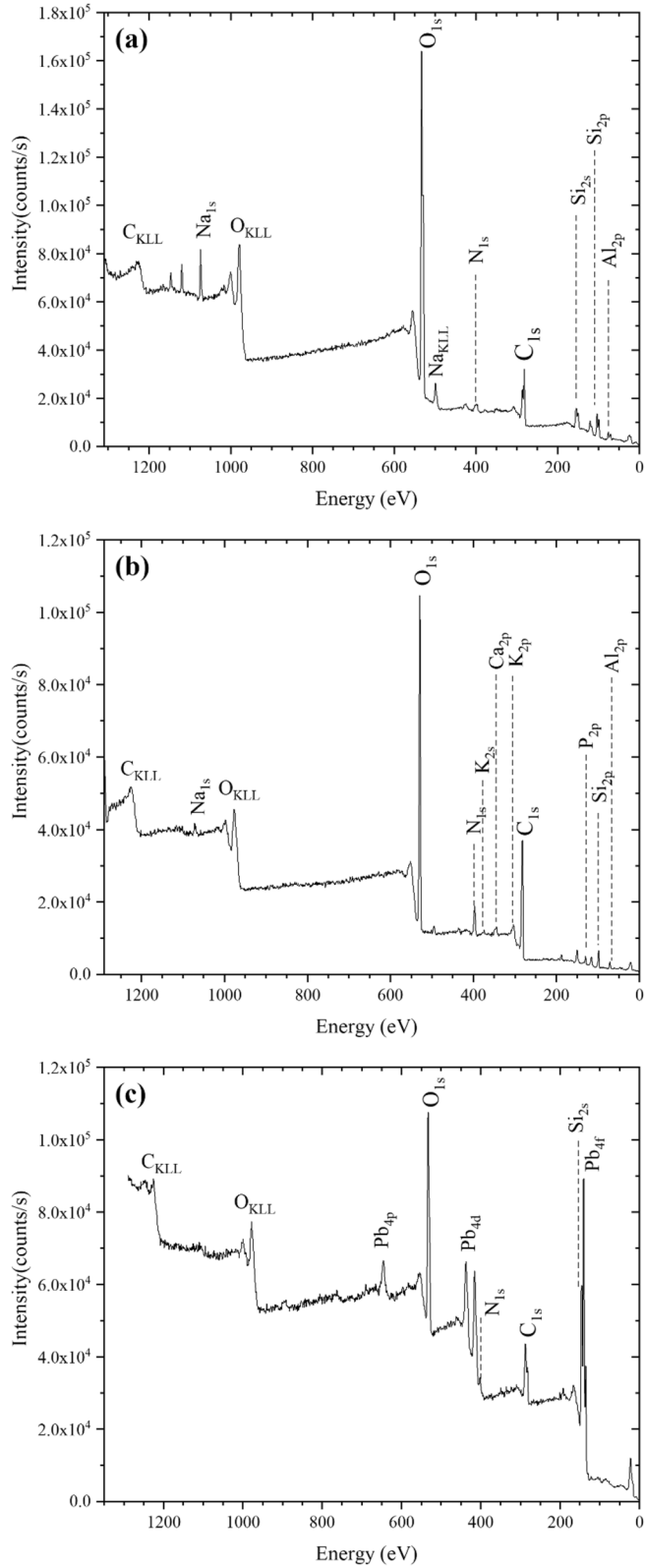

Fig. 8 Overall XPS survey spectra of geopolymer (**a**), JEONS5 (**b**), and Pb^{2+}-loaded JEONS5 (**c**)

Content courtesy of Springer Nature, terms of use apply. Rights reserved.

medium and the functional groups on the sorbent surface (Chen et al., 2022). The good fit of the equilibrium sorption data to the Langmuir isotherm model is consistent with monolayer-type Pb^{2+} uptake and the presence of energetically homogeneous sorption sites under the investigated conditions (Foo & Hameed, 2010). *E* value (< 16 kJ mol^{-1}) obtained from the D–R isotherm, together with the intensity decreases in Na^{+}, K^{+}, and Ca^{2+} signals observed by EDX after Pb^{2+} uptake, suggest that ion exchange may potentially contribute to the removal process (Akinterinwa et al., 2024; Iqbal et al., 2009). In addition, the shifts in FTIR bands corresponding to hydroxyl, amine, carbonyl, aluminosilicate, and Si–O-containing groups indicate the involvement of surface functional groups in Pb^{2+} removal. The EDTA regeneration results further support the presence of Pb–surface interactions. Overall, the available experimental evidence supports a multi-mechanistic interpretation of Pb^{2+} biosorption onto JEONS5, in which electrostatic interactions, ion exchange, and interactions with surface functional groups may act concurrently.

Conclusions

A new hybrid sorbent, JEONS5, was fabricated with a passive cell immobilization technique and employed to remove toxic Pb^{2+} ions from contaminated water. The combined action of *Neurospora* cells and the geopolymer matrix during the sorption process has been clearly demonstrated. JEONS5 has been successfully adapted for both batch and dynamic flow treatment systems to remove target heavy metal ions. The effective synthesis, combined action of the fungal cells and geopolymer matrix, and incorporation of functional groups, such as OH, –NH, C=O, C−N, Si–O, and Al–O, were validated by extensive analysis utilizing FTIR, SEM–EDX, XRD, XRF, and XPS. The sorption kinetics followed the PSO rate model and reached an equilibrium in 30 min. The Langmuir isotherm model best fit the equilibrium data, and the maximum sorption capacity was 217.56 ± 3.53 mg Pb^{2+} g^{-1}. The remarkable Pb^{2+} removal efficiency shown in studies using actual wastewater samples, along with its sorption and desorption performance during 20 consecutive cycles, suggests that JEONS5 may be a noteworthy option in the field. Moreover, temperature has no significant effect on the Pb^{2+} sorption pathway by JEONS5. The results of a fixed-bed column study also show that Chu's basic model fits the breakthrough curves well. The results of continuous and batch system testing conducted in a laboratory setting indicate that the proposed JEONS5 exhibits promising sorption effectiveness in both synthetic and real wastewater samples. However, several limitations should be considered. Sorption performance may be adversely impacted by competing metal ions and organic components, and industrial wastewaters may be more complicated than those examined here. Additionally, JEONS5's long-term mechanical stability and possible component leaching under extended regeneration circumstances have not been investigated in depth. Therefore, future research should focus on more complex, multi-component wastewater systems, pilot-scale feasibility studies, extended regeneration studies beyond 20 cycles, techno–economic and life cycle assessments, and AI-assisted application strategies. These investigations will make it more straightforward to implement the recommended material into practice.

Acknowledgements The Scientific and Technological Research Council of Türkiye (TÜBİTAK) provided funding for this study through Project No:123Y131. The authors gratefully acknowledge the financial support provided by TÜBİTAK.

Author contributions TA: Conceptualization, Methodology, Formal analysis, Resources, Writing—original draft. FS: Investigation, Data curation. STA: Resources, Formal analysis, Writing-review & editing. IK: Investigation, Resources. SC: Investigation, Data curation. HÇ: Investigation, Visualization. GÖ: Investigation, Visualization. FK: Supervision.

Funding Türkiye Bilimsel ve Teknolojik Araştırma Kurumu, Türkiye.

Data availability The authors declare that the main data supporting the findings of this study are available within the manuscript and its supplementary materials. Extra data are available on reasonable request from the corresponding author.

Declarations

Conflict of Interest The authors declare no conflict of interest.

References

Adebesin, B. O., Inyinbor, A. A., Oluyori, A., Adelani-Akande, T., Dada, A., & Oreofe, T. (2018). Water Pollution: Effects, Prevention, and Climatic Impact. In M. Glavan

Content courtesy of Springer Nature, terms of use apply. Rights reserved.

(Ed.), *Water Challenges of an Urbanizing World*. IntechOpen. https://doi.org/10.5772/intechopen.72018

Akar, T., Alim, S., Meltem, G., Sayin, F., & Tunali Akar, S. (2024). A novel sustainable and eco-friendly biosourced hybrid sorbent for toxic Pb^{2+} decontamination: Nano metal oxide functionalized salt-tolerant plant biomass. *Journal of Cleaner Production, 439*, Article 140838. https://doi.org/10.1016/j.jclepro.2024.140838

Akar, T., Celik, S., Gorgulu Ari, A., & Tunali Akar, S. (2013a). Removal of Pb^{2+} ions from contaminated solutions by microbial composite: Combined action of a soilborne fungus *Mucor plumbeus* and alunite matrix. *Chemical Engineering Journal, 215–216*, 626–634. https://doi.org/10.1016/j.cej.2012.11.001

Akar, T., Celik, S., Görgulu Ari, A., & Tunali Akar, S. (2013b). Nickel removal characteristics of an immobilized macro fungus: Equilibrium, kinetic and mechanism analysis of the biosorption. *Journal of Chemical Technology and Biotechnology, 88*(4), 680–689. https://doi.org/10.1002/jctb.3886

Akinterinwa, A., Oladele, E., Adebayo, A., & Adamu, M. (2024). Characterization of aqueous Pb2+ adsorption onto cross-linked-carboxymethyl legume starch phosphate using FTIR and SEM-EDX. *Biomass Conversion and Biorefinery, 14*(14), 16059–16073. https://doi.org/10.1007/s13399-023-03971-x

Aksu, Z., & Gönen, F. (2004). Biosorption of phenol by immobilized activated sludge in a continuous packed bed: Prediction of breakthrough curves. *Process Biochemistry, 39*(5), 599–613. https://doi.org/10.1016/S0032-9592(03)00132-8

Alabi, A. H., Adegoroye, A. C., Tella, F. O., Olanrewaju, C. A., Nnadozie, C. E., Mustapha, L. S., Oladoye, P. O., & Obayomi, K. S. (2026). In-situ synthesis of goethite-modified-*Albizia lebbeck* for sequestration of Zn^{2+} and Pb^{2+} from aqueous environments: Equilibrium, isotherm, and thermodynamic studies. *Cleaner Water, 5*, Article 100190. https://doi.org/10.1016/j.clwat.2025.100190

Blaga, A. C., Zaharia, C., & Suteu, D. (2021). Polysaccharides as support for microbial biomass-based adsorbents with applications in removal of heavy metals and dyes. *Polymers, 13*(17), Article 2893. https://doi.org/10.3390/polym13172893

Blanco, I., D'Angelo, A., Viola, V., Vertuccio, L., & Catauro, M. (2023). Metakaolin-based geopolymers filled with volcanic fly ashes: FT-IR, thermal characterization, and antibacterial property. *Science and Engineering of Composite Materials*. https://doi.org/10.1515/secm-2022-0192

Bouabidi, Z. B., El-Naas, M. H., & Zhang, Z. (2019). Immobilization of microbial cells for the biotreatment of wastewater: A review. *Environmental Chemistry Letters, 17*(1), 241–257. https://doi.org/10.1007/s10311-018-0795-7

Celik, S., Duman, N., Sayin, F., Tunali Akar, S., & Akar, T. (2021). Microbial cells immobilized on natural biomatrix as a new potential ecofriendly biosorbent for the biotreatment of reactive dye contamination. *Journal of Water Process Engineering, 39*, Article 101731. https://doi.org/10.1016/j.jwpe.2020.101731

Çelik, S., Tunali Akar, S., Şölener, M., & Akar, T. (2017). Anionically reinforced hydrogel network entrapped fungal cells for retention of cadmium in the contaminated aquatic media. *Journal of Environmental Management, 204*, 583–593. https://doi.org/10.1016/j.jenvman.2017.08.049

Chen, X., Li, J., & Yan, Z. (2026). Efficient heavy metal removal from aluminum alloy anodizing wastewater using a novel magnetic nanocomposite adsorbent. *Journal of Molecular Structure, 1351*, Article 144282. https://doi.org/10.1016/j.molstruc.2025.144282

Chen, Y., Wang, L., Hassan, M., Liu, Y., Wang, X., & Ren, D. (2022). Removal of aqueous lead ions by iron ore tailings/straw biochar composite and its underlying sorption mechanism. *Desalination and Water Treatment, 269*, 176–187. https://doi.org/10.5004/dwt.2022.28752

Chu, K. H. (2020). Breakthrough curve analysis by simplistic models of fixed bed adsorption: In defense of the century-old Bohart-Adams model. *Chemical Engineering Journal, 380*, Article 122513. https://doi.org/10.1016/j.cej.2019.122513

Das, M., & Adholeya, A. (2015). Potential uses of immobilized bacteria, fungi, algae, and their aggregates for treatment of organic and inorganic pollutants in wastewater. *Water challenges and solutions on a global scale* (Vol. Vol. 1206, pp. 319–337). American Chemical Society. https://doi.org/10.1021/bk-2015-1206.ch015

Davidovits, J. (1991). Geopolymers: Inorganic polymeric new materials. *Journal of Thermal Analysis and Calorimetry, 37*(8), 1633–1656. https://doi.org/10.1007/bf01912193

Ding, C., Cheng, W., Wang, X., Wu, Z.-Y., Sun, Y., Chen, C., Wang, X., & Yu, S.-H. (2016). Competitive sorption of Pb(II), Cu(II) and Ni(II) on carbonaceous nanofibers: A spectroscopic and modeling approach. *Journal of Hazardous Materials, 313*, 253–261. https://doi.org/10.1016/j.jhazmat.2016.04.002

Dou, S., Ke, X.-X., Shao, Z.-D., Zhong, L.-B., Zhao, Q.-B., & Zheng, Y.-M. (2022). Fish scale-based biochar with defined pore size and ultrahigh specific surface area for highly efficient adsorption of ciprofloxacin. *Chemosphere, 287*, Article 131962. https://doi.org/10.1016/j.chemosphere.2021.131962

Dubinin, M., & Radushkevich, L. (1947). Evaluation of microporous materials with a new isotherm. *Doklady Akademii Nauk SSSR, 55*, 331–334.

El Alouani, M., Saufi, H., Aouan, B., Bassam, R., Alehyen, S., Rachdi, Y., El Hadki, H., El Hadki, A., Mabrouki, J., Belaaouad, S., Ez-Zaki, H., & Barka, N. (2024). A comprehensive review of synthesis, characterization, and applications of aluminosilicate materials-based geopolymers. *Environmental Advances, 16*, Article 100524. https://doi.org/10.1016/j.envadv.2024.100524

Foo, K. Y., & Hameed, B. H. (2010). Insights into the modeling of adsorption isotherm systems. *Chemical Engineering Journal, 156*(1), 2–10. https://doi.org/10.1016/j.cej.2009.09.013

Gado, W. S., Morshedy, A. S., Entsar, Taha, H., El-Zahhar, A. A., Alghamdi, M. M., El Naggar, A. M. A., & El-Fawal, E. M. (2025). Efficient removal of cadmium ions from wastewater using metal oxide-doped sunflower stem-generated biochar: sorption mechanism and performance. *Biomass Conversion and Biorefinery*, *15*(24), 31245–31268. https://doi.org/10.1007/s13399-025-06845-6

Gupta, V. K., Ali, I., Saleh, T. A., Nayak, A., & Agarwal, S. (2012). Chemical treatment technologies for

Content courtesy of Springer Nature, terms of use apply. Rights reserved.

waste-water recycling—an overview. *RSC Advances, 2*(16), 6380–6388. https://doi.org/10.1039/c2ra20340e

Hammaini, A., González, F., Ballester, A., Blázquez, M. L., & Muñoz, J. A. (2007). Biosorption of heavy metals by activated sludge and their desorption characteristics. *Journal of Environmental Management, 84*(4), 419–426. https://doi.org/10.1016/j.jenvman.2006.06.015

Hammo, M. M., Akar, T., Sayin, F., Celik, S., & Akar, S. T. (2021). Efficacy of green waste-derived biochar for lead removal from aqueous systems: Characterization, equilibrium, kinetic and application. *Journal of Environmental Management, 289*, Article 112490. https://doi.org/10.1016/j.jenvman.2021.112490

Han, R., Zou, L., Zhao, X., Xu, Y., Xu, F., Li, Y., & Wang, Y. (2009). Characterization and properties of iron oxide-coated zeolite as adsorbent for removal of copper(II) from solution in fixed bed column. *Chemical Engineering Journal, 149*(1), 123–131. https://doi.org/10.1016/j.cej.2008.10.015

Ho, Y. S., & McKay, G. (1999). Pseudo-second order model for sorption processes. *Process Biochemistry, 34*(5), 451–465. https://doi.org/10.1016/S0032-9592(98)00112-5

Hong, M. S., Ong, W.-J., Oh, K. S., Chan, E.-S., & Lam, W. H. (2026). Core-shell Ca-alginate beads formed via inverse-gelation technique for the enhanced removal of lead(II) from aqueous solution. *International Journal of Biological Macromolecules, 337*, Article 149481. https://doi.org/10.1016/j.ijbiomac.2025.149481

Iqbal, M., Saeed, A., & Zafar, S. I. (2009). FTIR spectrophotometry, kinetics and adsorption isotherms modeling, ion exchange, and EDX analysis for understanding the mechanism of Cd^{2+} and Pb^{2+} removal by mango peel waste. *Journal of Hazardous Materials, 164*(1), 161–171. https://doi.org/10.1016/j.jhazmat.2008.07.141

Kara, I., Tunc, D., Sayin, F., & Akar, S. T. (2018). Study on the performance of metakaolin based geopolymer for Mn(II) and Co(II) removal. *Applied Clay Science, 161*, 184–193. https://doi.org/10.1016/j.clay.2018.04.027

Kara, İ, Yilmazer, D., & Akar, S. T. (2017). Metakaolin based geopolymer as an effective adsorbent for adsorption of zinc(II) and nickel(II) ions from aqueous solutions. *Applied Clay Science, 139*, 54–63. https://doi.org/10.1016/j.clay.2017.01.008

Kumar, R., Kumar Joshi, H., Vishwakarma, M. C., Sharma, H., Joshi, S. K., & Bhandari, N. S. (2023). Biosorption of copper and lead ions onto treated biomass *Myrica esculenta*: Isotherms and kinetics studies. *Environmental Nanotechnology, Monitoring & Management, 19*, Article 100775. https://doi.org/10.1016/j.enmm.2022.100775

Kümmerer, K., Dionysiou, D. D., Olsson, O., & Fatta-Kassinos, D. (2018). A path to clean water. *Science, 361*(6399), 222–224. https://doi.org/10.1126/science.aau2405

Lagergren, S. (1898). Zur theorie der sogenannten adsorption geloster stoffe, Kungliga svenska vetenskapsakademiens. *Handlingar, 24*, 1–39.

Lan, T., Li, P., Rehman, F. U., Li, X., Yang, W., & Guo, S. (2019). Efficient adsorption of Cd^{2+} from aqueous solution using metakaolin geopolymers. *Environmental Science and Pollution Research, 26*(32), 33555–33567. https://doi.org/10.1007/s11356-019-06362-w

Lester, E., Hilal, N., & Henderson, J. (2004). Porosity in ancient glass from Syria (c. 800 AD) using gas adsorption and atomic force microscopy. *Surface and Interface Analysis, 36*(9), 1323–1329. https://doi.org/10.1002/sia.1911

Low, K. S., Lee, C. K., & Liew, S. C. (2000). Sorption of cadmium and lead from aqueous solutions by spent grain. *Process Biochemistry, 36*(1), 59–64. https://doi.org/10.1016/S0032-9592(00)00177-1

Luhar, I., Luhar, S., Abdullah, M. M. A. B., Razak, R. A., Vizureanu, P., Sandu, A. V., & Matasaru, P.-D. (2021). A state-of-the-art review on innovative geopolymer composites designed for water and wastewater treatment. *Materials, 14*(23), 7456. https://doi.org/10.3390/ma14237456

Najim, A. A., Radeef, A. Y., al-Doori, I., & Jabbar, Z. H. (2024). Immobilization: The promising technique to protect and increase the efficiency of microorganisms to remove contaminants. *Journal of Chemical Technology and Biotechnology, 99*(8), 1707–1733. https://doi.org/10.1002/jctb.7638

Olatunji, M. A., Salam, K. A., & Evuti, A. M. (2024). Continuous removal of Pb (II) and Cu (II) ions from synthetic aqueous solutions in a fixed-bed packed column with surfactant-modified activated carbon. *Separation Science and Technology, 59*(4), 561–579. https://doi.org/10.1080/01496395.2024.2329790

Pakshirajan, K., & Swaminathan, T. (2006). Continuous biosorption of Pb, Cu, and Cd by *Phanerochaete chrysosporium* in a packed column reactor. *Soil and Sediment Contamination: An International Journal, 15*, 187–197. https://doi.org/10.1080/15320380500506347

Ramteke, L. P., & Gogate, P. R. (2016). Treatment of water containing heavy metals using a novel approach of immobilized modified sludge biomass based adsorbents. *Separation and Purification Technology, 163*, 215–227. https://doi.org/10.1016/j.seppur.2016.02.047

Sayin, F., Tunali Akar, S., Akar, T., Celik, S., & Gedikbey, T. (2021). Chitosan immobilization and Fe_3O_4 functionalization of olive pomace: An eco–friendly and recyclable Pb^{2+} biosorbent. *Carbohydrate Polymers, 269*, Article 118266. https://doi.org/10.1016/j.carbpol.2021.118266

Shojaosadati, S. A., Faraidouni, R., Madadi-Nouei, A., & Mohamadpour, I. (1999). Protein enrichment of lignocellulosic substrates by solid state fermentation using *Neurospora sitophila*. *Resources, Conservation and Recycling, 27*(1), 73–87. https://doi.org/10.1016/S0921-3449(98)00086-X

Suter, E., Rutto, H., & Omwoyo, W. (2025). Continuous packed bed column removal of Cr^{6+}, Cd^{2+}, and Pb^{2+} ions from synthetic wastewater using polymeric ultra-permeable and biodegradable ferromagnetic nanocomposite membrane. *Canadian Journal of Chemical Engineering, 103*(6), 2642–2658. https://doi.org/10.1002/cjce.25555

Tan, P., Sun, J., Hu, Y., Fang, Z., Bi, Q., Chen, Y., & Cheng, J. (2015). Adsorption of Cu^{2+}, Cd^{2+} and Ni^{2+} from aqueous single metal solutions on graphene oxide membranes. *Journal of Hazardous Materials, 297*, 251–260. https://doi.org/10.1016/j.jhazmat.2015.04.068

Tyagi, U. (2022). Enhanced adsorption of metal ions onto *Vetiveria zizanioides* biochar via batch and fixed bed studies. *Bioresource Technology, 345*, Article 126475. https://doi.org/10.1016/j.biortech.2021.126475

Content courtesy of Springer Nature, terms of use apply. Rights reserved.

Ungureanu, G., Enache, I.-M., Cara, I. G., Motrescu, I., & Patras, A. (2024). Insights into the environmental benefits of using apple pomace for biosorption of lead from contaminated water. *Heliyon, 10*(17), Article e36811. https://doi.org/10.1016/j.heliyon.2024.e36811

Verma, M., Lee, I., Sharma, S., Kumar, R., Kumar, V., & Kim, H. (2021). Simultaneous removal of heavy metals and ciprofloxacin micropollutants from wastewater using ethylenediaminetetraacetic acid-functionalized β-cyclodextrin-chitosan adsorbent. *ACS Omega, 6*(50), 34624–34634. https://doi.org/10.1021/acsomega.1c05015

Vijayaraghavan, K., & Yun, Y.-S. (2008). Bacterial biosorbents and biosorption. *Biotechnology Advances, 26*(3), 266–291. https://doi.org/10.1016/j.biotechadv.2008.02.002

Volesky, B. (1990). Removal and recovery of heavy metals by biosorption. In B. Volesky (Ed.), *Biosorption of heavy metals* (pp. 7–43). CRC press.

Wang, Y., Yu, W., Han, J., You, C., Zhang, X., Liu, Z., & Wu, Z. (2025). Biosorption characteristics and Caco-2 cells detoxification evaluations of lead(II) using exopolysaccharides produced by *Paenibacillus bovis* BD3526 in a wheat-bran medium. *Environmental Technology & Innovation, 37*, Article 104059. https://doi.org/10.1016/j.eti.2025.104059

Wei, E., Wang, K., Muhammad, Y., Chen, S., Dong, D., Wei, Y., & Fujita, T. (2022). Preparation and conversion mechanism of different geopolymer-based zeolite microspheres and their adsorption properties for Pb^{2+}. *Separation and Purification Technology, 282*, Article 119971. https://doi.org/10.1016/j.seppur.2021.119971

Wu, C., Zhi, D., Yao, B., Zhou, Y., Yang, Y., & Zhou, Y. (2022). Immobilization of microbes on biochar for water and soil remediation: A review. *Environmental Research, 212*, Article 113226. https://doi.org/10.1016/j.envres.2022.113226

Younis, M. Y., Li, W., Khan, J., & Wei, Y. (2025). Lotus carbon dots doped sodium alginate hydrogel beads for effective adsorptive removal of Cd^{2+} and potential application in Pb^{2+} removal from wastewater. *International Journal of Biological Macromolecules, 322*, Article 146638. https://doi.org/10.1016/j.ijbiomac.2025.146638

Zeldowitsch, J. (1934). Über den mechanismus der katalytischen oxydation von CO an MnO_2. *Acta Physicochimica U.R.S.S., 1*, 364–449.

Zhang, B., Yu, T., Deng, L., Li, Y., Guo, H., Zhou, J., Li, L., & Peng, Y. (2022). Ion-adsorption type rare earth tailings for preparation of alkali-based geopolymer with capacity for heavy metals immobilization. *Cement and Concrete Composites, 134*, Article 104768. https://doi.org/10.1016/j.cemconcomp.2022.104768

Zhang, Y., Yuan, K., Magagnin, L., Wu, X., Jiang, Z., & Wang, W. (2023a). Schiff base functionalized silica aerogels for enhanced removal of Pb (II) and Cu (II): Performances, DFT calculations and LCA analysis. *Chemical Engineering Journal, 462*, Article 142019. https://doi.org/10.1016/j.cej.2023.142019

Zhang, Z., Liu, N., Li, X., Wang, Y., Xiong, Y., Meng, R., Liu, L., & He, S. (2023b). Single-step hydrothermal synthesis of biochar from waste industrial hemp stalk core for Pb^{2+} sorption: Characterization and mechanism studies. *Sustainable Chemistry and Pharmacy, 36*, Article 101316. https://doi.org/10.1016/j.scp.2023.101316

Zhao, C., Li, X., Ding, C., Liao, J., Du, L., Yang, J., Yang, Y., Zhang, D., Tang, J., Liu, N., & Sun, Q. (2016). Characterization of uranium bioaccumulation on a fungal isolate *Geotrichum* sp. dwc-1 as investigated by FTIR, TEM and XPS. *Journal of Radioanalytical and Nuclear Chemistry, 310*(1), 165–175. https://doi.org/10.1007/s10967-016-4797-2

Publisher's Note Springer Nature remains neutral with regard to jurisdictional claims in published maps and institutional affiliations.

Springer Nature or its licensor (e.g. a society or other partner) holds exclusive rights to this article under a publishing agreement with the author(s) or other rightsholder(s); author self-archiving of the accepted manuscript version of this article is solely governed by the terms of such publishing agreement and applicable law.

Content courtesy of Springer Nature, terms of use apply. Rights reserved.

Terms and Conditions

Springer Nature journal content, brought to you courtesy of Springer Nature Customer Service Center GmbH ("Springer Nature").
Springer Nature supports a reasonable amount of sharing of research papers by authors, subscribers and authorised users ("Users"), for small-scale personal, non-commercial use provided that all copyright, trade and service marks and other proprietary notices are maintained. By accessing, sharing, receiving or otherwise using the Springer Nature journal content you agree to these terms of use ("Terms"). For these purposes, Springer Nature considers academic use (by researchers and students) to be non-commercial.
These Terms are supplementary and will apply in addition to any applicable website terms and conditions, a relevant site licence or a personal subscription. These Terms will prevail over any conflict or ambiguity with regards to the relevant terms, a site licence or a personal subscription (to the extent of the conflict or ambiguity only). For Creative Commons-licensed articles, the terms of the Creative Commons license used will apply.
We collect and use personal data to provide access to the Springer Nature journal content. We may also use these personal data internally within ResearchGate and Springer Nature and as agreed share it, in an anonymised way, for purposes of tracking, analysis and reporting. We will not otherwise disclose your personal data outside the ResearchGate or the Springer Nature group of companies unless we have your permission as detailed in the Privacy Policy.
While Users may use the Springer Nature journal content for small scale, personal non-commercial use, it is important to note that Users may not:

1. use such content for the purpose of providing other users with access on a regular or large scale basis or as a means to circumvent access control;
2. use such content where to do so would be considered a criminal or statutory offence in any jurisdiction, or gives rise to civil liability, or is otherwise unlawful;
3. falsely or misleadingly imply or suggest endorsement, approval , sponsorship, or association unless explicitly agreed to by Springer Nature in writing;
4. use bots or other automated methods to access the content or redirect messages
5. override any security feature or exclusionary protocol; or
6. share the content in order to create substitute for Springer Nature products or services or a systematic database of Springer Nature journal content.

In line with the restriction against commercial use, Springer Nature does not permit the creation of a product or service that creates revenue, royalties, rent or income from our content or its inclusion as part of a paid for service or for other commercial gain. Springer Nature journal content cannot be used for inter-library loans and librarians may not upload Springer Nature journal content on a large scale into their, or any other, institutional repository.
These terms of use are reviewed regularly and may be amended at any time. Springer Nature is not obligated to publish any information or content on this website and may remove it or features or functionality at our sole discretion, at any time with or without notice. Springer Nature may revoke this licence to you at any time and remove access to any copies of the Springer Nature journal content which have been saved.
To the fullest extent permitted by law, Springer Nature makes no warranties, representations or guarantees to Users, either express or implied with respect to the Springer nature journal content and all parties disclaim and waive any implied warranties or warranties imposed by law, including merchantability or fitness for any particular purpose.
Please note that these rights do not automatically extend to content, data or other material published by Springer Nature that may be licensed from third parties.
If you would like to use or distribute our Springer Nature journal content to a wider audience or on a regular basis or in any other manner not expressly permitted by these Terms, please contact Springer Nature at

onlineservice@springernature.com